lated from the empirical path occupancy rate r_i by the following relation:

$$\lambda_n = \frac{r_n}{(K-1)r_{n-1}+1} \qquad n \neq 1$$

where $\lambda_1 = r_1$. The path number distribution is then calculated successively, using the recursive formulas given for this model in Reference 6. Figs. 4 and 5 show a comparison between the empirical path number distributions and the modified Poisson distributions for the manufacturing floors and college campuses, respectively. The curve fittings show considerable improvement over those of the Poisson model.

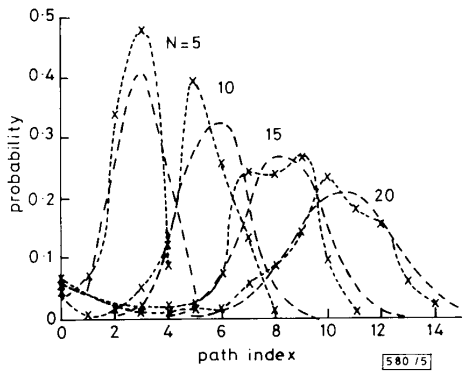

Fig. 5 *Comparison of empirical and modified Poisson distribution for college laboratory areas*

This improvement is because the modified Poisson model utilises the empirical probability of occupancy for each bin, whereas the Poisson model just uses the sum of the probabilities of occupancy for all bins. The optimum values of K calculated for the manufacturing floors and the campus environments are shown in Table 1.

Table 1 OPTIMUM VALUES OF K

Area	Number of locations	Number of bins N			
		5	10	15	20
Manufacturing floors	288	1·184	0·904	1·03	2·46
College laboratories	196	0·892	0·64	0·61	0·75

Conclusions: Fading multipath profiles obtained from several different manufacturing floors and some college laboratories at 910 MHz, have been used to model the arrival of the paths. The empirical distribution was compared with the Poisson and the modified Poisson distributions and the modified Poisson model is shown to provide a better fit. This observation indicates that the paths tend to arrive in clusters rather than in a random manner.

Acknowledgment: This work was supported in part by the National Science Foundation under contract NCR-8703435.

R. GANESH
K. PAHLAVAN

Department of Electrical Engineering
Worcester Polytechnic Institute
Worcester, MA 01609, USA

8th March 1989

References

1 PAHLAVAN, K., GANESH, R., and HOTALING, T.: 'Multipath propagation measurements on manufacturing floors at 910 MHz', *Electron. Lett.*, 1989, **25**, pp. 225–227

2 DEVASIRVATHAM, D. M. J.: 'Time delay spread measurements of 850 MHz radio waves in building environments'. GLOBECOM 1985 Conf. Rec., vol. 2, Dec. 1985, pp. 970–973

3 BULTITUDE, R. J. C., MAHMOUD, S. A., and SULLIVAN, W. A.: 'A comparison of indoor radio propagation characteristics at 910 MHz and 1·75 GHz'. *IEEE JSAC*, Jan. 1988, pp. 20–30

4 SALEH, A. A. M., and VALENZUELA, R. A.: 'A statistical model for indoor multipath propagation'. *IEEE JSAC*, Feb. 1987, pp. 128–137

5 PAHLAVAN, K.: 'Wireless intra-office networks', *ACM Trans. Off. Inf. Syst.*, 1988, (2)

6 SUZUKI, H.: 'A statistical model for urban radio propagation', *IEEE Trans. Commun.*, 1977, **COM-25**

7 TURIN, G. L., CLAPP, F. D., JOHNSTON, T. L., FINE, S. B., and LAVRY, D.: 'A statistical model of urban multipath propagation', *IEEE Trans. Veh. Technol.*, 1972, (1), pp. 1–9

10 MHz CMOS OTA-C VOLTAGE-CONTROLLED QUADRATURE OSCILLATOR

Indexing terms: Circuit theory and design, Oscillators, Integrated circuits, Nonlinear networks

A quadrature-type voltage-controlled oscillator with operational transconductance amplifiers and capacitors (OTA-C) is presented. A monolithic integrated CMOS test circuit is introduced to verify theoretical results. The attainable frequency range of oscillation of the chip test circuit is 3–10·34 MHz. The total harmonic distortion (THD) is 0·20–1·87% for corresponding peak-to-peak amplitude voltages between 100 mV and 1 V. This amplitude can be controlled either by using a diode connection of two MOS transistors or a proposed nonlinear resistor.

Introduction: The quadrature mode of operation is a well-known mode of waveform generation in the field of sinewave oscillators.[1–3] Two sinewaves in quadrature, that is with 90° phase difference, are generated. This is accomplished with a two-integrator loop. Besides this, some form of regeneration is usually included to ensure that the oscillation is created. The poles are initially located in the right half-plane (RHP) of the complex frequency plane and then pulled back by a nonlinear amplitude limiter.

To make a quadrature oscillator into a voltage-controlled oscillator (VCO), the integrators can be implemented using OTAs. The output current of a CMOS-OTA is controlled by the differential input voltage and its transconductance gain g_m. Furthermore, g_m can be varied over several octaves by adjusting an external DC amplifier bias current I_{abc},[4] i.e.

$$g_m = h_C\sqrt{(I_{abc})} \tag{1}$$

where h_C is a process-dependent parameter.

In this letter an integrated CMOS OTA-C quadrature VCO using a 3 μm double metal technology (processed by MOSIS, Marina del Rey, CA) is presented. The frequency of oscillation can be externally adjusted by nearly two octaves with a THD less than 1·9%. The real part of the poles can be adjusted, in practice, independently of the frequency of oscillation.

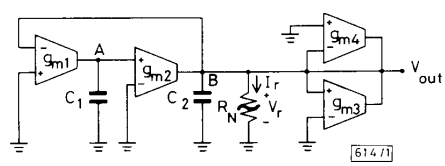

Fig. 1 *Proposed OTA-C quadrature oscillator structure*

Theory: The proposed quadrature VCO architecture[5] is shown in Fig. 1. It has one inverting (g_{m1}, C_1) and one noninverting integrator (g_{m2}, C_2). R_N is a nonlinear resistor whose i/v characteristics are depicted in Fig. 2*a*. R_N provides the nonlinear amplitude limiter function. Implementations are discussed later. The OTAs associated with g_{m3} and g_{m4} allow

placing the poles in the RHP. The characteristic equation of the oscillator is given by

$$s^2 + \frac{s}{C_2}[GN(A) - (g_{m3} - g_{m4})] + \frac{g_{m1}g_{m2}}{C_1C_2} = 0 \qquad (2)$$

where $GN(A)$ is the equivalent conductance of R_N using the describing function.[6] Thus, for $V_r(t) = A \cos \omega t$ and $i_r = f_r(V_r)$, it yields

$$N(A) = \frac{1}{AT}\int_0^T \frac{f_r(A \cos \omega t) \cos \omega t}{G}\, dt \qquad (3)$$

where $T = 2\pi/\omega$. For a transfer characteristic as shown in Fig. 2*a*, we obtain

$$N(A) = 0 \qquad \text{for } A \ll E \qquad (4a)$$

$$N(A) = 1 \qquad \text{for } A \gg E \qquad (4b)$$

therefore, when $A = 0$ and making $g_{m3} > g_{m4}$, the roots of eqn. 2 are in the RHP and the oscillator will be self-starting. As the amplitude of oscillation increases $GN(A)$ also increases, and the roots are pulled back toward the imaginary axis.

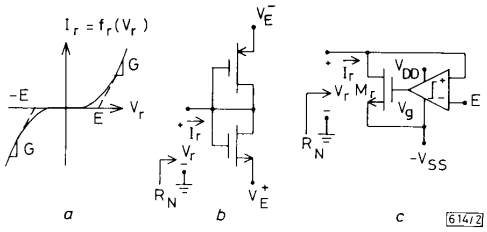

Fig. 2 *Nonlinear resistor*

a i/v characteristics
b Simple R_N implementation
c Proposed nonlinear resistor

Furthermore, when $GN(A) = g_{m3} - g_{m4}$, it is guaranteed that the roots will reach the imaginary axis for some value of A and hence a stable limit cycle is reached. This cycle is characterised by

$$\omega = \sqrt{\left(\frac{g_{m1}g_{m2}}{C_1C_2}\right)} \qquad (5)$$

$$A = N^{-1}\left[\frac{g_{m3} - g_{m4}}{G}\right] \qquad (6)$$

CMOS implementations of R_N: Two alternatives are discussed; the first one, shown in Fig. 2*b*, is simply a diode connection of two MOS transistors. For the second implementation the principle of operation is illustrated in Fig. 2*c*. If $V_r < E$ then $V_g = -V_{SS}$ and transistor M_r is in cutoff ($i_r = 0$). If $V_r > E$, V_g becomes positive and M_r is on and capable of driving a large current. For implementing the complete characteristic of Fig. 2*a*, a similar circuit (Fig. 2*c*) is added, with M_r being a PMOS. Since the performance of the comparator is not critical, a simple differential input to a single-ended output amplifier[4] is used.

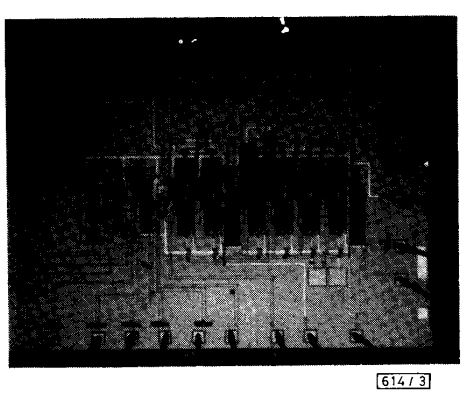

Fig. 3 *Photomicrograph of test chip*

Experimental results: A 3 μm CMOS process (through and thanks to MOSIS) test prototype was fabricated. The capacitors C_1 and C_2 were not physically implemented, instead the parasitic capacitances associated with nodes A and B of Fig. 1 were used. Fig. 3 shows a photomicrograph of the test chip. The linearised OTA used is similar to the one presented by Nedungadi and Geiger[7] with transconductance increased by a factor of four. The range of the g_ms of the OTA is 8–238 μmho. For an output amplitude of 1 V peak-to-peak, the frequency range is 3 to 10·34 MHz, and the THD is kept below 2%. When reducing the oscillation amplitude, the distortion is lowered, i.e. for 100 mV peak-to-peak, the measured THD at 10 MHz was 0·2%. Fig. 4 shows the measured spectrum for an oscillation frequency of 10 MHz and 1 V peak-to-peak amplitude, using a nonlinear resistor implementation based on Fig. 2*c*.

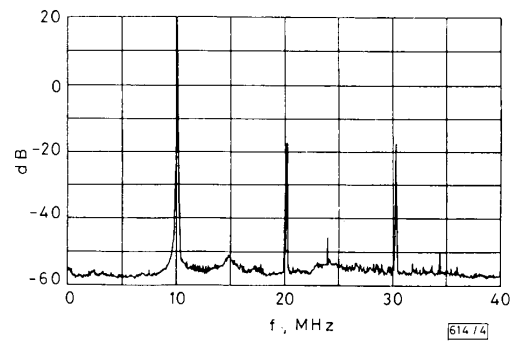

Fig. 4 *Spectrum of $V_{out} = 1\,V \times (2\pi \times 10^7)$ using R_N of Fig. 2c*

Conclusions: A versatile voltage-controlled OTA-C quadrature oscillator with a novel nonlinear amplitude limiter has been introduced. An experimental trade-off between THD and the amplitude of the oscillating sinewave has been shown. A good high-frequency range was obtained using a conventional 3 μm CMOS (double-metal) process. The voltage-control property makes it possible to have the oscillator tuned on chip for different applications and/or temperature and process variations. The proposed OTA-C oscillator architecture has potential to operate at higher frequencies by using a better CMOS process and/or an improved OTA design.

B. LINARES-BARRANCO*†
A. RODRÍGUEZ-VÁZQUEZ†
E. SÁNCHEZ-SINENCIO*
J. L. HUERTAS†

13th March 1989

**Department of Electrical Engineering*
Texas A&M University
College Station, TX 77843, USA

†Dpto. Electrónica y Electromagnetismo
Fac. Física
Universidad de Sevilla
41012 Seville, Spain

References

1 SEDRA, A. S., and SMITH, K. C.: 'Microelectronic circuits' (Holt, Rinehart and Winston, 1987), 2nd edition
2 HOYLE, J., and SÁNCHEZ-SINENCIO, E.: 'Sinusoidal quadrature oscillators'. 27th Midwest Symposium on Circuits and Systems, 1984, pp. 59–62
3 GRAEME, J. G., TOBEY, G. E., and HUELSMAN, L. P.: 'Operational amplifiers design and applications' (McGraw-Hill, 1971), pp. 385–391
4 ALLEN, P. E., and HOLBERG, R. D.: 'CMOS analog circuit design' (Holt, Rinehart and Winston, 1987)
5 LINARES-BARRANCO, B., RODRÍGUEZ-VÁZQUEZ, A., HUERTAS, J. L., SÁNCHEZ-SINENCIO, E., and HOYLE, J. J.: 'Generation and design of sinusoidal oscillators using OTA's'. Proc. IEEE/ISCAS, 1988, 3, pp. 2863–2866

6 GELB, A., and VANDER VELDE, W.: 'Multiple-input describing functions and non-linear system design' (McGraw-Hill, 1968)
7 NEDUNGADI, A., and GEIGER, R. L.: 'High-frequency voltage-controlled continuous-time lowpass filter using linearised CMOS integrators', *Electron. Lett.*, 1986, **22**, pp. 729–730

COMPRESSION AND DISPERSIONLESS TRANSMISSION OF CHIRPED 1·3 μm DFB ps LASER PULSES IN DISPERSION-SHIFTED SINGLE-MODE FIBRES

Indexing terms: Optical communications, Semiconductor lasers, Optical dispersion, Optical transmission

Optical pulse compression of high-speed gain-switched ps 1·3 μm DFB semiconductor laser pulses in dispersion-shifted single-mode fibres is measured with a streak camera. The laser red-shift chirp is compensated for by the negative chromatic fibre dispersion, resulting in pulse compression and 'dispersionless' transmission of 45 ps pulses over 12 km of fibre.

Introduction: Optical wavelength chirping of the individual longitudinal modes of a gain-switched or high-speed modulated semiconductor laser has been previously observed in time-resolved studies.[1–4] The chirp-induced dispersion penalty is one of the important factors which eventually limits the high-speed transmission of DFB laser signals. Several schemes have been proposed to reduce chirp in DFB lasers for high-speed transmission in dispersive fibres. The use of external modulation, modulation-pulse-shapening, CW-injection locking and special reduced-chirp laser cavity designs have been reported. An entirely different approach, instead of trying to eliminate the chirp, is to control the chirp and use it to advantage in fibre transmission. We report the experimental realisation of an earlier proposal[5] which utilises the chirped DFB laser pulse compression to achieve 'dispersionless' transmission in dispersion-shifted single-mode fibres (DS-SMF). In this scheme, the fibre's dispersion is negative at the laser wavelength and so longer wavelengths propagate faster and the red-shift chirp is compensated for, resulting in pulse compression and subsequent rebroadening in the fibre. The fibre distance over which the optical input pulse is initially compressed and later rebroadened to its input pulse width is called the 'dispersionless' distance L_0.[5] We report measurements of L_0 in DS-SMF using high-speed ps pulses from a 1·3 μm DFB laser.[5–8]

Experiment: The experimental set-up is shown in Fig. 1. The DFB laser is gain-switched with the signal from the comb generator, which is driven by a sinewave (1, 2 or 3 GHz) of 5–8 V amplitude, providing output pulse widths in the 23–45 ps range (simulating 10–20 Gbit/s modulation speeds). The wavelength and threshold current of the laser are $\lambda_S = 1{\cdot}29\,\mu m$ and $I_{th} = 29{\cdot}0$ mA, respectively. The optical signal is detected by a Hamamatsu synchroscan streak camera (rise time <10 ps). The DS-SMF dispersion is −22 ps/nm/km at $\lambda_S = 1{\cdot}29\,\mu m$ with the zero dispersion at $\lambda_0 = 1{\cdot}55\,\mu m$. At 1, 2 and 3 GHz repetition rates the laser was biased at $I_{DC} = 30{\cdot}4$, 36·8 and 41·3 mA and modulated with $I_{pp} = 155$, 92, and 46 mA, resulting in peak powers of 5·4, 4·2 and 2·7 mW, respectively, in the fibre pigtail. Fig. 2 shows the pulse waveforms at various fibre lengths for the 3 GHz repetition rate. It is seen that the initial laser pulse (FWHM = 45 ps) is compressed to 15 ps after transmission over 5 km of fibre after which it starts to rebroaden. After transmission over 10·5 and 14·0 km of fibre a shoulder appears in the pulse due to the overtaking of the 'red' wavelengths in the beginning of the pulse. Fig. 3 shows the pulse width variation against the fibre length and the total dispersion for the three pulse repetition rates. The dispersionless transmission distance for the 3 GHz pulses is $L_0 = 12$ km. The results of these measurements are consistent with theoretical results.[5,6] For a laser with λ_S closer to λ_0, say $\lambda_S = 1{\cdot}53\,\mu m$, the dispersionless distance becomes 156 km. This is simply because a longer fibre length is required to compensate for the much smaller fibre dispersion at 1·53 μm, and the transmission then becomes loss-limited. Fig. 3 also shows that L_0 increases with the pulse width. This is due to a smaller chirp width at the higher repetition rates, which is attributed to the lower pump currents in our particular case. As a consequence, a broader optical pulse with a smaller chirp width of 0·30 nm (−6 dB down) is obtained at 3 GHz, as compared with the chirp widths of 1·20 and 0·85 nm at 1 and 2 GHz, respectively. We also examined the effect of decreasing the bias current at 3 GHz modulation. This resulted in a significantly larger chirp width. In addition we noticed the effect of lowering the pump current for the case of

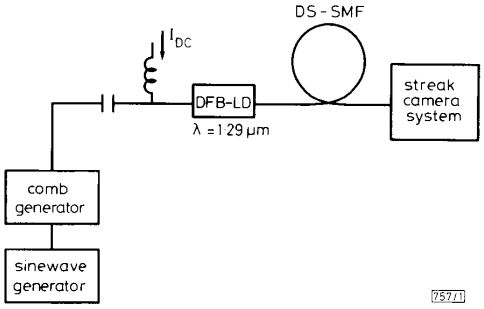

Fig. 1 *Experimental set-up for pulse compression measurements*

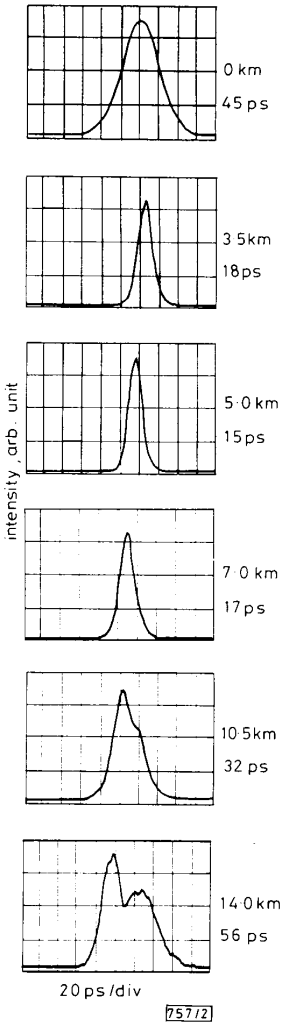

Fig. 2 *Optical pulse waveforms after transmission over various lengths of fibre at 3 GHz*